Chemical Science

ROYAL SOCIETY OF CHEMISTRY

EDGE ARTICLE

View Article Online
View Journal | View Issue



Cite this: *Chem. Sci.*, 2024, **15**, 10508

All publication charges for this article have been paid for by the Royal Society of Chemistry

Received 12th January 2024
Accepted 28th May 2024

DOI: 10.1039/d4sc00267a

rsc.li/chemical-science

# Hsp90α forms condensate engaging client proteins with RG motif repeats†

Jiaojiao Hu, *[ab] Hui Dong,[ab] Yichen Li,[c] Jinge Gu,[ab] Liang Yang,[de] Chenfang Si,[a] Yaoyang Zhang,[a] Tingting Li,[de] Dan Li*[cf] and Cong Liu *[ab]

Hsp90α, a pivotal canonical chaperone, is renowned for its broad interaction with numerous protein clients to maintain protein homeostasis, chromatin remodeling, and cell growth. Recent studies indicate its role in modifying various components of membraneless organelles (MLOs) such as stress granules and processing bodies, suggesting its participation in the regulation of protein condensates. In this study, we found that Hsp90α possesses an inherent ability to form dynamic condensates *in vitro*. Utilizing LC-MS/MS, we further pinpointed proteins in cell lysates that preferentially integrate into Hsp90α condensates. Significantly, we observed a prevalence of RG motif repeats in client proteins of Hsp90α condensates, many of which are linked to various MLOs. Moreover, each of the three domains of Hsp90α was found to undergo phase separation, with numerous solvent-exposed negatively charged residues on these domains being crucial for driving Hsp90α condensation through multivalent weak electrostatic interactions. Additionally, various clients like TDP-43 and hnRNPA1, along with poly-GR and PR dipeptide repeats, exhibit varied impacts on the dynamic behavior of Hsp90α condensates. Our study spotlights various client proteins associated with Hsp90α condensates, illustrating its intricate adaptive nature in interacting with diverse clients and its functional adaptability across multiple MLOs.



## Introduction

Molecular chaperones play a critical role in ensuring protein translation and proper folding while preventing the misfolding and aggregation of proteins that can lead to cellular malfunction.[1–5] Among these, Hsp90 and Hsp70 have been extensively studied, with Hsp90 involved in the folding and activation of a diverse array of client proteins such as kinases, steroid hormone receptors, and transcription factors.[6–8] Hsp70 primarily assists in the folding of new polypeptides, the repair of denatured proteins, and the targeted destruction of faulty proteins.[9] Together with co-chaperones like the Hsp40 family, these chaperones are vital for maintaining protein homeostasis.[10–13] Disruptions in these chaperone-mediated processes have been associated with a variety of diseases, including cancer, neurodegenerative disorders, and metabolic issues.[14–16] Specifically, Hsp90 and its co-chaperones are increasingly acknowledged as crucial in the molecular mechanisms of neurodegenerative diseases like Alzheimer's and Parkinson's diseases.[17,18]

Recent studies have shown that several chaperones, including Hsp70 and Hsp40, have a strong ability to undergo phase separation and play a significant role in maintaining the protein homeostasis within MLOs such as stress granules, nuclear bodies, and P-bodies.[19–21] This highlights the importance of chaperones in maintaining the functional integrity of MLOs and preventing protein aggregation. For example, Hsp70 has been shown to engage in phase separation, contributing to the maintenance of the liquidity and functional dynamics of TDP-43 nuclear bodies and preventing TDP-43 aggregation.[22,23] Similarly, in stress granules, Hsp70 helps prevent the solidification of TDP-43 and FUS.[23,24] Notably, Hsp90 has been identified as a stress granules' regulator, where it stabilizes other components and is involved in the disassembly of stress granules and the regulation of SC35 speckles during mitosis with the help of co-chaperone DYRK3.[25–27] Therefore, exploring whether Hsp90 is capable of phase separation and how it interacts with its client proteins in condensates is crucial for understanding its role in regulating various MLOs.

In this study, we demonstrate that Hsp90α undergoes phase separation *in vitro* and characterized its phase separation profile

[a]*Interdisciplinary Research Center on Biology and Chemistry, Shanghai Institute of Organic Chemistry, Chinese Academy of Sciences, Shanghai 201210, China. E-mail: hujj@sioc.ac.cn; liulab@sioc.ac.cn*

[b]*State Key Laboratory of Chemical Biology, Shanghai Institute of Organic Chemistry, Chinese Academy of Sciences, Shanghai, 200032, China*

[c]*Bio-X Institutes, Key Laboratory for the Genetics of Developmental and Neuropsychiatric Disorders, Ministry of Education, Shanghai Jiao Tong University, Shanghai 200240, China. E-mail: lidan2017@sjtu.edu.cn*

[d]*Department of Biomedical Informatics, School of Basic Medical Sciences, Peking University Health Science Center, Beijing 100191, China*

[e]*Key Laboratory for Neuroscience, Ministry of Education, National Health Commission of China, Peking University, Beijing 100191, China*

[f]*Zhangjiang Institute for Advanced Study, Shanghai Jiao Tong University, Shanghai 200240, China*

† Electronic supplementary information (ESI) available. See DOI: https://doi.org/10.1039/d4sc00267a

by using a high-throughput protein phase separation (HiPPS) profiling assay. We found that proteins enriched in reconstituted Hsp90α condensates from mammalian cell lysates typically contain RG motif repeats. Our further investigations indicate that the phase separation of Hsp90α is driven by its negatively charged surface of the three individual domains. Interestingly, we found that dipeptide repeats of $GR_n$ or $PR_n$, as caused by the mutations in C9orf72 gene, significantly alter the dynamics of Hsp90α condensates, in contrast to the minimal impact of other client proteins including TDP-43 and hnRNPA1. Our study not only sheds light on the *in vitro* phase separation characteristics of Hsp90α but also enhances our understanding of the regulatory mechanism of Hsp90α condensate by different client proteins.

## Results

### Hsp90α exhibits phase separation ability *in vitro*

We first sought to explore the capability of Hsp90α for condensate formation *in vitro*. To achieve this, we overexpressed and purified Hsp90α to a high degree of purity and subjected it to a high-throughput protein phase separation (HiPPS) profiling assay, which we had previously developed.[28] This assay was designed to systematically evaluate the liquid–liquid phase separation characteristics of different proteins. We incorporated a variety of factors into this screening, including diverse crowding agents, salt concentrations, charged polymers, and buffer pH levels, all arranged within a 96-well plate (Fig. S1a†). Upon adding Hsp90α and thoroughly mixing, we performed microscopic imaging of the plate. Notably, Hsp90α demonstrated the formation of distinctive, round-edged droplets under over twenty distinct conditions, especially in environments containing polyR peptides (like $CR_7$ and $CR_{20}$) and crowding agents (such as PEG 8000 and PEG 3350) at certain pH levels (Fig. 1a and S1b†). Utilizing a specific grading criterion for the microscopic images from the HiPPS profiling, we determined a phase separation score of 3.1 (at 25 μM concentration) for Hsp90α (Fig. 1b), indicating a relatively modest condensation propensity compared to other phase-separated proteins previously studied.[28] The radar chart derived from HiPPS profiles highlighted those conditions in the blue zone, particularly those with polyR peptides, were most conducive to promoting Hsp90α condensation (Fig. 1c).

We then prepared fluorescent dye-labeled Hsp90α and examined its phase separation behavior with the addition of PEG 8000 and $CR_{20}$. Through differential interference contrast (DIC) and fluorescence microscopy, we confirmed droplet formation of Hsp90α with 10% (v/w) PEG 8000. Fluorescence recovery after photobleaching (FRAP) assays showed that about 50% of the fluorescent intensity recovered within roughly 500 seconds, demonstrating the formation of dynamic Hsp90α condensates (Fig. 1d). In the presence of $CR_{20}$, Hsp90α also condensed into droplets (Fig. 1e), yet the dynamics of these condensate were notably different, showing a slower fluorescent intensity recovery rate of about 30% in 500 seconds. Collectively, these findings confirm that Hsp90α can undergo phase separation *in vitro*, and that different agents distinctly influence the internal dynamics of Hsp90α condensates.

### Reconstituted Hsp90α condensates recruited client proteins containing RG motifs

Given Hsp90α's ability to form condensates, we aimed to identify the specific client proteins that are preferentially incorporated into Hsp90α condensates within a cellular environment. To investigate the protein interactions of Hsp90α within these condensates, we established an *in vitro* cell lysate system that allows us to replicate, modify, and closely study the phase separation behavior of Hsp90α (Fig. 2a). In brief, HeLa cells were harvested and lysed in a minimal buffer, then centrifuged to eliminate cell debris. The clear supernatant, containing a mix of cytoplasmic and nuclear elements, served as our cell lysate. This lysate, confirmed to be free of visible condensates or irregularities by DIC imaging (Fig. S2†), was used in subsequent experiments. Once we introduced Hsp90α and PEG 8000 into this cell lysate, spherical droplets formed. As a control, the cell lysate dopped with Hsp90α protein doesn't form droplet in the absence of PEG 8000 (Fig. S3†).

We then conducted a detailed investigation of the proteins incorporated into the Hsp90α-mediated lysate condensates using mass spectrometry. Specifically, we utilized liquid chromatography-tandem mass spectrometry (LC-MS/MS) to profile the proteins within the condensate formed whenHsp90α concentration was increased by 20 μM. A parallel lysate sample with the same Hsp90α concentration but without PEG 8000 served as a control (Fig. S3†). This analysis resulted in identifying 515 proteins that were significantly more prevalent in the Hsp90α condensate compared to the control, with Hsp90α itself being the most abundant, confirming its primary role in the condensate (Fig. 2b and Table S1†).

Gene ontology analysis highlighted a significant presence of these client proteins in functions related to chaperone and RNA binding within the Hsp90α condensate. These proteins were notably involved in RNA metabolism processes, including processing, translation, and splicing (Fig. 2c and Table S2†). Remarkably, further analysis using the PhaSepDB database revealed that 411 out of 515 identified client proteins were involved in various MLOs, such as stress granules, Cajal bodies, and nuclear bodies, suggesting Hsp90α's role in maintaining protein homeostasis in these MLOs (Fig. 2d and Table S3†).[29] Moreover, motif analysis of the proteins enriched in the Hsp90α condensate showed a dominance of arginine–glycine motifs (RG motifs), including RG, GR, GRG, RGR, RRG, GRR, and RGG (Fig. 2e and Table S4†). Among proteins with RG motifs, 179 proteins contain RG-motif repeats (at less two RG motif) (Fig. 2f). Meanwhile, other motifs, including the FG and QN motifs, did not exhibit any particular preference in the Hsp90α condensates (Fig. S4†). This observation aligns with our HiPPS results showing that $CR_{20}$ is potent in promoting Hsp90α condensation, suggesting that multivalent weak electrostatic interactions may play an important role in mediating co-condensation of Hsp90α and its client proteins. Overall, our results indicate that Hsp90α selectively recruits client proteins with RG-motifs repeats, which play roles across different MLOs.

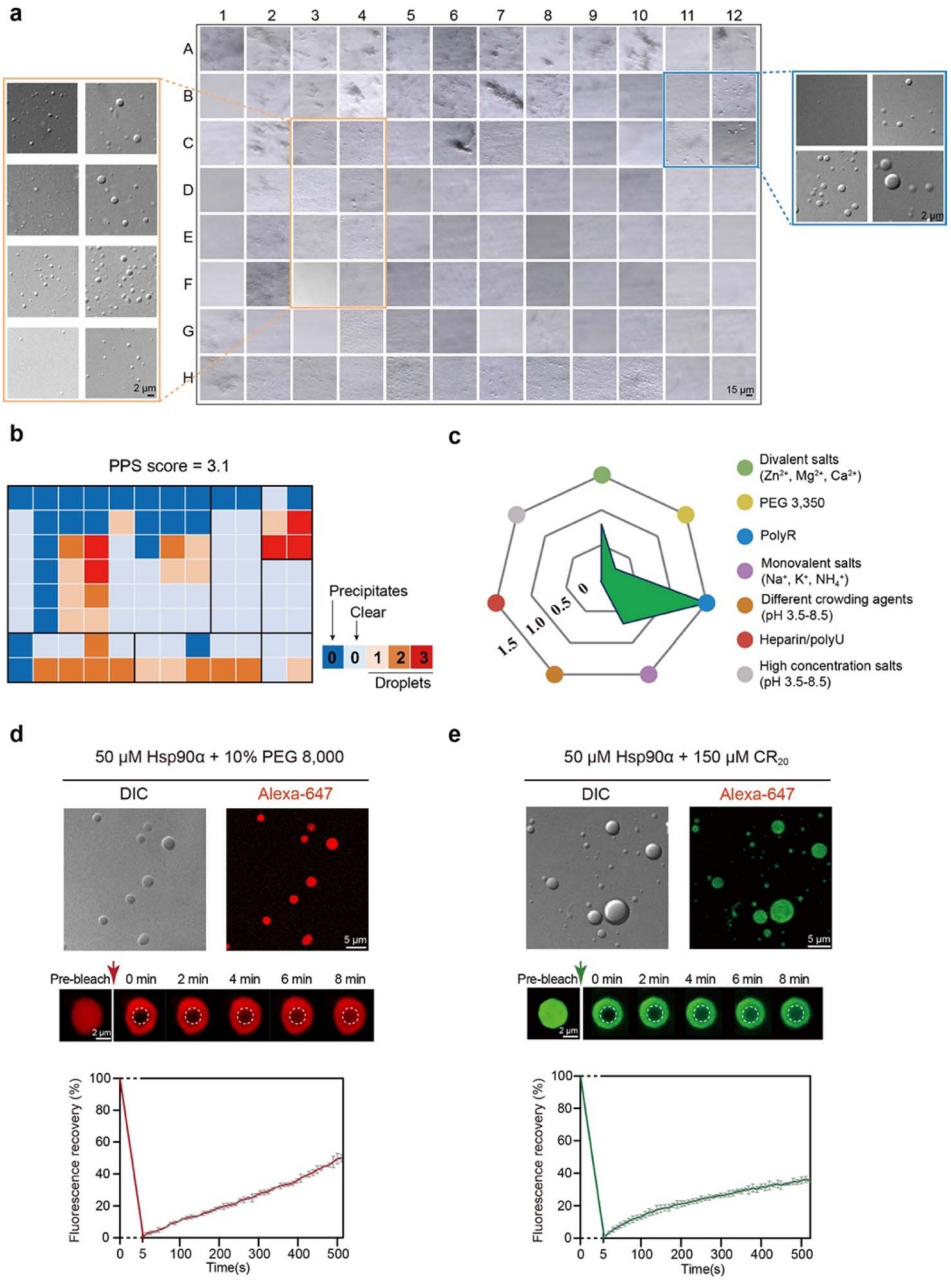


Fig. 1 Profiling *in vitro* phase separation of Hsp90α by HiPPS. (a) Microscopic images of HiPPS profiling for 25 μMHsp90α in the bright-field mode. Zoom in, DIC images for wells C3–F4 and B11–C12. (b) The HiPPS profile of 25 μM Hsp90α. The wells are graded and colored based on their microscopic images according to the grading criteria described previously. (c) Values of the average grades of each color zone in the HiPPS profiles. (d) DIC and fluorescence images of Hsp90α condensation under indicated conditions (top). FRAP measurement of Hsp90α droplets in 50 μM Hsp90α, pH 7.5, 100 mM NaCl, and 10% PEG 8000. Data shown are mean ± SEM, $n = 3$. Data are from three independent bleaching experiments. (e) DIC and fluorescence images of Hsp90α condensation with the addition of 150 μM $CR_{20}$ (top). FRAP measurement of Hsp90α droplets in 50 μM Hsp90α, 150 μM $CR_{20}$, pH 7.5, 100 mM NaCl. Data shown are mean ± SEM, $n = 3$. Data are from three independent bleaching experiments.

## Negatively charged residues is essential to mediate Hsp90α condensation

We then aimed to elucidate the contribution of each domain to Hsp90α condensation. Hsp90α is composed of three highly conserved regions: the N-terminal domain (NTD), which is known for ATP binding, the middle domain (MD), and the C-terminal domain (CTD), which is crucial for dimerization (Fig. 3a). We purified the NTD, MD, and CTD of Hsp90α and assessed their capacity for phase separation in comparison to the full-length (FL) Hsp90α, using $CR_{20}$ to simulate the conditions of its co-phase separating client proteins. Surprisingly, we observed that each domain individually could form condensates, though their phase separation was significantly less pronounced than that of

bleaching experiments.

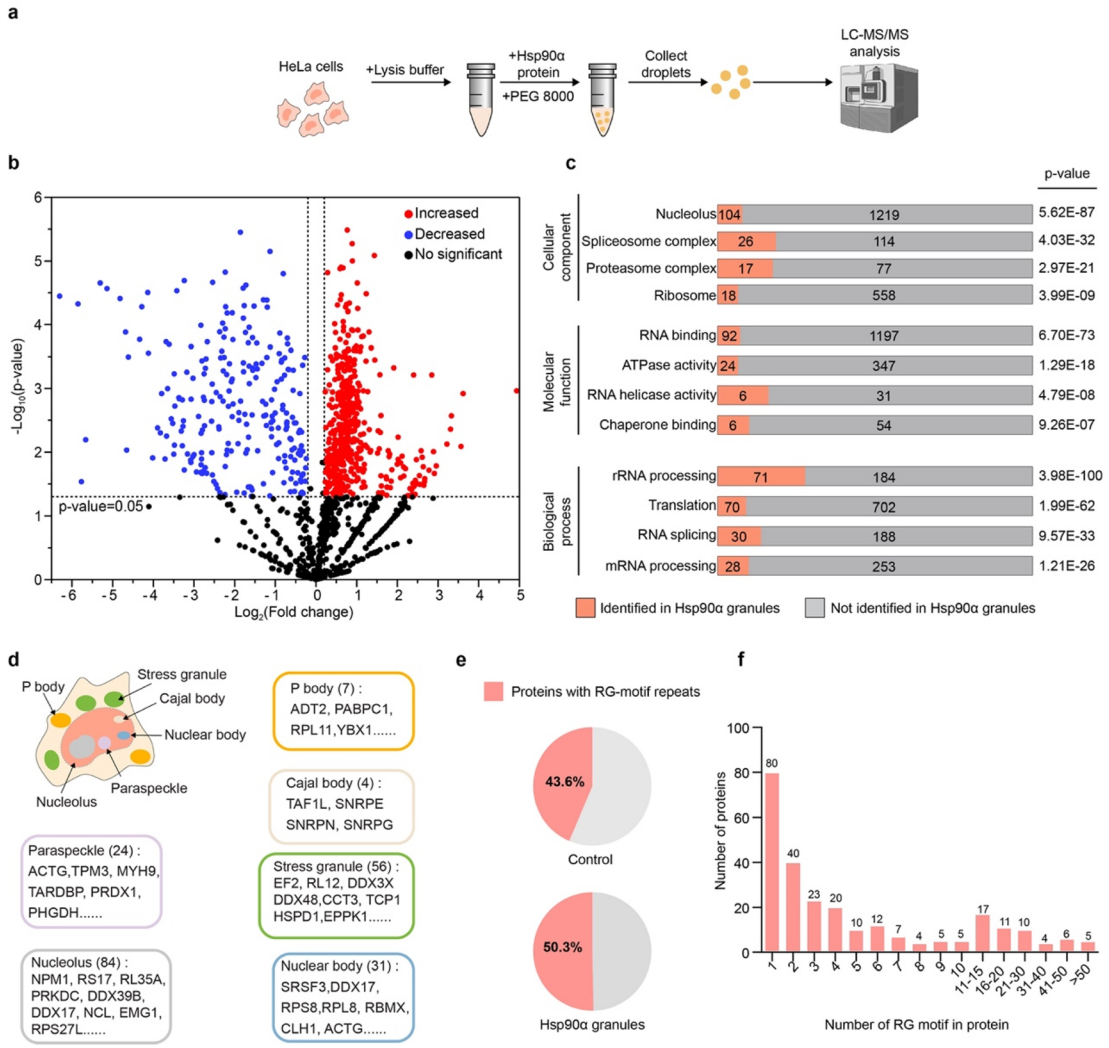


Fig. 2 Proteomic analysis showing Hsp90α condensate containing proteins with RG motifs. (a) Schematic illustrating the generation and proteomic analysis of Hsp90α granules from cell lysates. (b) Volcano plot displaying protein enrichment in Hsp90α granules *versus* control, with significant changes highlighted in red (increased) and blue (decreased). (c) Gene ontology analysis of enriched proteins in Hsp90α granules. (d) Schematic of a cell with membrane less organelles related to enriched proteins in Hsp90α granules. (e) Percentage of RG motif-containing proteins within the Hsp90α granules compared to percentage of RG motif-containing proteins in the control. (f) The number of RG motifs in the client proteins of Hsp90α granules.

the FL Hsp90α, as evidenced by the turbidity measurements of the condensate samples (Fig. 3b and c). This suggests that all three domains contribute to Hsp90α's condensation.

Further structural analysis of Hsp90α revealed numerous negatively charged residues on the surfaces of Hsp90α's NTD, MD, and CTD, specifically E62, D66, D156, D157, E158 on the NTD, D302, D303, E307, E308, E311, E553, D554, E555, E556, E557 on the MD, and D699, E700, D701, D702, D706, D707 on the CTD (Fig. 3d). Considering that multivalent weak electrostatic interactions are believed to be crucial for the co-condensation of Hsp90α and its client proteins, we hypothesized that these surface-exposed negatively charged residues might play a significant role in facilitating Hsp90α condensation. To investigate this, we replaced the surface-exposed Glu and Asp residues with Ala in each domain (Fig. 3e). Structural alignments indicated that modifying these residues resulted in slight changes to the structures of NTD, MD and CTD (Fig. S5†). Remarkably, altering these residues in the NTD and MD eliminated their ability to undergo phase separation in the presence of 50 μM $CR_{20}$ and significantly reduced their phase separation at higher concentrations of $CR_{20}$ (100 μM and 150 μM). Furthermore, mutating the CTD completely negated its phase separation ability, even with 150 μM $CR_{20}$ added. These findings reinforce the model that the multiple negatively charged residues on the solvent-exposed surfaces of the three domains are pivotal in driving Hsp90α condensation through multivalent electrostatic interactions with multiple arginine residues from its client proteins.

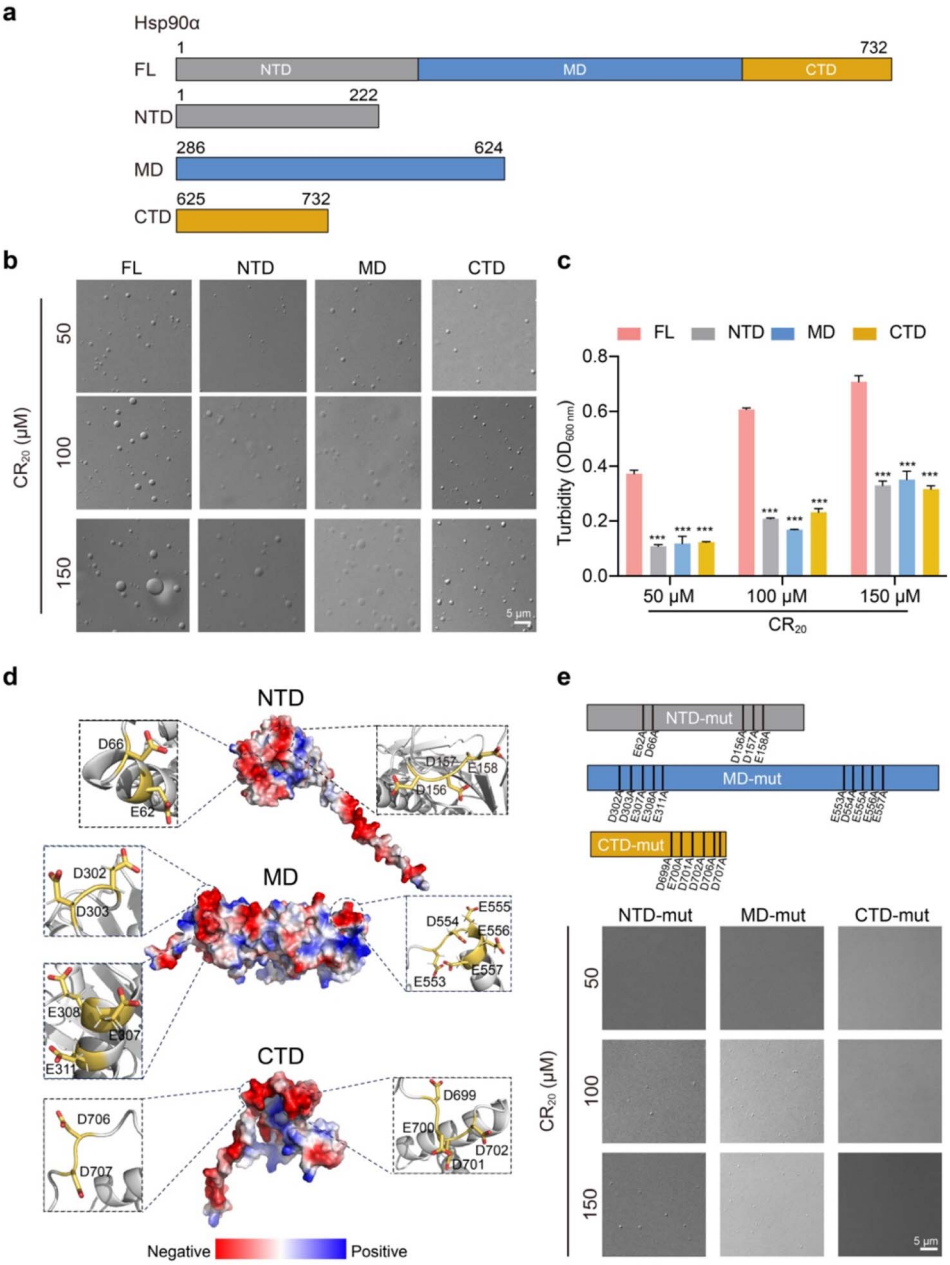


Fig. 3 Characterization of phase separation by Hsp90α and its variants. (a) Domain organization of Hsp90α WT and truncated variants. (b) DIC and fluorescence images of 50 μM Hsp90α WT and variant condensate with the addition of varied concentrations of $CR_{20}$ in the buffer containing 50 mM Tris, pH 7.5, 100 mM NaCl. (c) Turbidity measurement of Hsp90α FL and truncations in the addition of varying concentrations of $CR_{20}$. Data shown are mean ± SD, $n = 3$. ***, $p < 0.001$. (d) Electrostatic surface representation of Hsp90α (structure generated by AlphaFold 2). The key negatively charged residues are shown in zoomed-in view. (e) DIC images for the condensation of 50 μM Hsp90α mutations in the addition of varied concentrations of $CR_{20}$ in the buffer containing 50 mM Tris, pH 7.5, 100 mM NaCl.

### Different client proteins distinctively alter Hsp90α condensates dynamics

Since Hsp90α condensates have the capacity to incorporate client proteins with various RG motifs, we proceeded to explore how different RG-motif client proteins might in turn affect the phase separation behavior of Hsp90α. We selected two client proteins that were notably enriched in the Hsp90α-induced lysate condensate, TDP-43, and hnRNPA1 (Table S1†). The direct binding of hnRNPA1 and TDP-43 was validated by the biolayer interferon (BLI) assay (Fig. S6†). Both TDP-43 and hnRNPA1 are RNA-binding proteins, previously recognized for their ability to phase separate *in vitro* and within cells.[23,30,31] The abnormal condensation of TDP-43 and hnRNPA1 has been implicated in neurodegenerative diseases like Amyotrophic Lateral Sclerosis (ALS) and Frontotemporal Lobar Degeneration (FTLD).[32–35] As shown in Fig. 4a and b, these proteins co-phase separate with Hsp90α, corroborating the proteomics results of the Hsp90α condensate. Of note, we utilized PEG 8000 instead

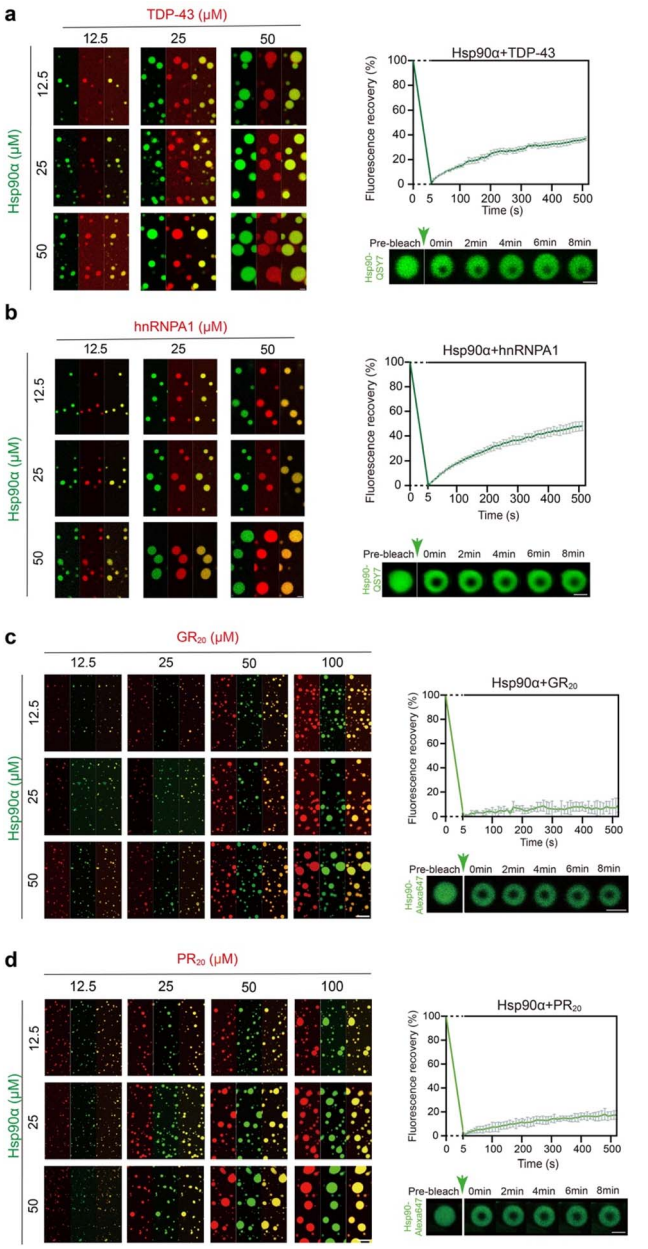


Fig. 4 The co-phase separation of Hsp90α and the four different RG motifs containing client proteins *in vitro*. (a) Fluorescence images of co-condensation of Hsp90α and TDP-43 (left). Scale bar, 5 μm. FRAP of droplets formed by 50 μM Hsp90α and 50 μM TDP-43 (right) in 50 mM Tris, pH 7.5, 100 mM NaCl, and 10% PEG 8000. Scale bar, 2 μm. (b) Fluorescence images of co-condensation of Hsp90α and hnRNPA1 (left). Scale bar, 5 μm. FRAP of droplets formed by 50 μM Hsp90α and 50 μM hnRNPA1 (right) in 50 mM Tris, pH 7.5, 100 mM NaCl, and 10% PEG 8000. Scale bar, 2 μm. (c) Fluorescence images of co-phase separation of Hsp90α and $GR_{20}$ (left). Scale bar, 5 μm. FRAP of droplets formed by 50 μM Hsp90α and 50 μM $GR_{20}$ (right) in 50 mM Tris, pH 7.5, 100 mM NaCl. Scale bar, 2 μm. (d) Fluorescence images of co-phase separation of Hsp90α and $PR_{20}$ (left). Scale bar, 5 μm. FRAP of droplets formed by 50 μM Hsp90α and 50 μM $PR_{20}$ (right) in 50 mM Tris, pH 7.5, 100 mM NaCl. Scale bar, 2 μm. The FRAP curves shown in (a)–(d) represents the recovery of Hsp90α fluorescence, with data presented as mean ± SEM, $n = 3$. Data are from three independent bleaching experiments.

of $CR_{20}$ to induce Hsp90α condensation to eliminate any potential effects from the arginine residues in $CR_{20}$. Furthermore, the addition of both client proteins significantly enhanced the phase separation of Hsp90α (Fig. 4a and b). However, FRAP analysis revealed that incorporating TDP-43 and hnRNPA1 had a minimal impact on the internal dynamics of the droplets compared to those formed solely by Hsp90α (Fig. 4a, b and 1d).

Recent study has identified $GR_{50}$ and $PR_{50}$ dipeptide repeats produced through repeat-associated non-ATG (RAN) translation associated with C9orf72, as major contributors to the pathogenesis of C9-ALS/FTD.[36–38] Significantly, Hsp90α has been detected in the interactomes of these toxic dipeptide repeats, suggesting they may serve as Hsp90α clients under disease conditions.[39,40] The direct interaction of $GR_{20}$ and $PR_{20}$ to Hsp90α was first determined by BLI assay. The result showed that $GR_{20}$ and $PR_{20}$ exhibit extensive binding to Hsp90α, with $K_D$ of 8.97 ± 0.11 nM and 9.08 ± 0.19 nM, respectively (Fig. S7†). Thus, we introduced $GR_{20}$ and $PR_{20}$ dipeptide repeats to assess their impact on Hsp90α condensation. Remarkably, both $GR_{20}$ and $PR_{20}$ were able to co-phase separate with Hsp90α (Fig. 4c and d). The formation of larger Hsp90α condensates was observed with increasing concentrations of $GR_{20}$ and $PR_{20}$, indicating that these clients promote Hsp90α phase separation. Strikingly, Hsp90α condensates demonstrated significantly reduced fluorescence recovery (less than 20% in approximately 500 seconds) after bleaching when $GR_{20}$ and $PR_{20}$ peptides were introduced, suggesting that these pathological clients markedly impair the internal dynamics of Hsp90α condensates upon co-phase separation with Hsp90α (Fig. 4c and d). In summary, our findings indicate that client proteins with different RG motif patterns can co-phase separate with Hsp90α and enhance its condensation. Furthermore, various clients distinctly influence the internal dynamics of Hsp90α condensates.

## Discussion

Recently, Hsp90α has gained attention for its regulatory influence on the components of stress granules and processing bodies, underscoring its potential in modulating protein clients within phase-separated states.[41–43] In our study, we demonstrated that Hsp90α can undergo phase separation *in vitro* and comprehensively characterized the interactome of Hsp90α within this phase-separated condition. Notably, we discovered that the protein clients of Hsp90α in the condensate are primarily linked to various MLOs and contain multiple RG motif repeats. It is known that in humans, over 1700 proteins contain at least two RG motif repeats within a stretch of fewer than five residues.[44] The initial discovery of RG repeats in the mid-1980s came from the study of proteins such as the adenovirus hexon-assembly protein, nucleolin, and fibrillarin.[45–48] However, there has been a recent resurgence in interest regarding the phase separation capabilities of proteins with RG motif repeats.[49] Often found in low-complexity domains, as in G3BP1, TDP-43, and FUS, these locally enriched RG motif repeats are important in facilitating protein condensation and interacting with RNA, influencing the phase separation

behavior within the condensate.[50–52] Our work suggests that Hsp90α can engage various client proteins within the condensate through interactions with these RG motifs, potentially offering a common mechanism for how Hsp90α manages a broad array of client proteins across different MLOs.

Interestingly, our findings indicate that client proteins with varying RG motif repeats can distinctly affect the dynamics of the Hsp90α condensates. This implies that the co-condensation of Hsp90α with different clients may result in unique properties, reflecting diverse functions in various MLOs. Nevertheless, further research is necessary to unravel the specific mechanisms by which Hsp90α recognizes and interacts with different client proteins across various MLOs, ensuring protein homeostasis and the functional integrity of the MLOs. Notably, we observed that the pathological client protein, GR and PR dipeptide repeats, enhances Hsp90α condensation and significantly impairs the internal dynamics of condensates. This could potentially trap Hsp90α in a solid-like condensates, hindering its physiological functions in the cell and leading to a disruption of protein homeostasis. This insight offers a novel perspective on understanding the mechanisms behind poly-GR dipeptide repeats-mediated ALS pathology.

## Materials and methods

### Plasmid construction

For *E. coli* expression, gene of full-length human Hsp90α (UniProt accession number P07900) was inserted into pET28a vector with a N-terminal 6×-His tag. The Hsp90α NTD (1–222), MD (286–624), and CTD (625–732) were generated from Hsp90α WT, respectively, and further subcloned into pET28a with an N-terminal 6×-His tag. The NTD, MD and CTD mutations were generated by site-directed mutagenesis of the wild-type vector using the Phanta Max Super-Fidelity DNA Polymerase kit (Vazyme, P505). The sequences of all constructs were verified by GENEWIZ from Azenta Life Science (Suzhou, China). Genes of the TDP-43 and hnRNPA1 were used as previously described.[28,53]

### Peptide synthesis

The $CR_{20}$, $GR_{20}$, and $PR_{20}$ were synthesized by ChinaPeptides Co., Ltd (Shanghai, China). Freeze-dried peptides were dissolved in $ddH_2O$ or buffer containing 50 mM Tris–HCl, pH 7.5, 100 mM NaCl for HiPPS profiling assay and *in vitro* LLPS assays, respectively.

### Protein expression and purification

Hsp90α and mutations including NTD, MD, CTD, NTD-mut, MD-mut, and CTD-mut were overexpressed in BL21 (DE3) Chemically Competent Cells (Transgene, CD601). Expression of protein was induced by adding 1 mM isopropyl β-D-thiogalactoside (IPTG), and cells were cultured at 16 °C overnight. Cells were harvested and lysed in 50 mM Tris–HCl, pH 7.5, 500 mM NaCl, 4 mM β-mercaptoethanol, 5% (v/v) glycerol, and 2 mM PMSF. The cell lysates were centrifuged and filtered before loading onto the Ni column. Proteins were then eluted with buffer containing 50 mM Tris–HCl, pH 7.5, 500 mM NaCl, 100 mM imidazole, 4 mM β-mercaptoethanol, and 5% glycerol. Eluted fractions were further purified by using the size exclusion chromatography (Superdex 200 16/600, GE Healthcare) in buffer containing 50 mM Tris–HCl, pH 7.5, 100 mM NaCl, 2 mM DTT. For NTD, MD, CTD and their mutations, the size exclusion chromatography (Superdex 75 16/600, GE Healthcare) was applied.

TDP-43 was overexpressed in BL21 (DE3) pLysS Chemically Competent Cells (Transgene, CD701). Expression of protein was induced by adding 1 mM IPTG, and cells were cultured at 16 °C overnight. Cells were harvested and lysed in 50 mM Tris–HCl, pH 7.5, 1 M NaCl, 2 mM DTT, 10% (v/v) glycerol, 1 mM EDTA, and 2 mM PMSF. RNase A (Roche, 10109169001) was added into the lysis buffer to remove RNA. The cell lysates were centrifuged and filtered before loading onto the MBP Trap HP column. Proteins were then eluted with 50 mM Tris–HCl, pH 7.5, 1 M NaCl, 2 mM DTT, 10% glycerol, and 10 mM maltose. Eluted fractions were further purified by using the size exclusion chromatography (Superdex 200 16/600, GE Healthcare) in buffer containing 50 mM Tris–HCl, pH 7.5, 300 mM NaCl, 2 mM DTT.

hnRNPA1 was overexpressed in BL21 (DE3) pLysS Chemically Competent Cells (Transgene, CD701). Expression of protein was induced by adding 0.4 mM IPTG, and cells were cultured at 25 °C overnight. Cells were harvested and lysed in 50 mM Tris–HCl, pH 7.5, 2 mM DTT, and 2 mM PMSF. RNase A (Roche, 10109169001) was added into the lysis buffer to remove RNA. The cell lysates were centrifuged and filtered before loading onto the SP FF column. Proteins were then eluted with 50 mM Tris–HCl, pH 7.5, 1 M NaCl. Eluted fractions were further purified by using the size exclusion chromatography (Superdex 75 16/600, GE Healthcare) in buffer containing 50 mM Tris–HCl, pH 7.5, 500 mM NaCl, 2 mM DTT. All purified proteins were stored at −80 °C before use.

The fluorescent dyes, modified by succinimidyl esters, were used to label the primary amines on the surfaces of proteins. Initially, the proteins were desalted into a reaction buffer consisting of 50 mM PB, pH 7.5, 300 mM NaCl, and 2 mM DTT. Subsequently, the proteins were incubated with a two-fold molar excess of fluorescent dye, specifically Alexa Fluor 488 (Invitrogen, A20100) for $CR_{20}$, $GR_{20}$, $PR_{20}$, TDP-43, and hnRNPA1, and Alexa Fluor 647 (Invitrogen, A20006) for Hsp90α. The labeling reaction was carried out for one hour at room temperature. Afterwards, the labeled proteins were further purified using either Superdex 75 10/300 columns or Superdex 200 10/300 columns (GE Healthcare, USA).

### *In vitro* high-throughput protein phase separation (HiPPS) profiling assay

For the HiPPS profiling assay, stock solutions containing 96 different LLPS-inducing reagents (detailed in Table S1†), were prepared and stored separately. Aliquots of these solutions were allocated into a 96-well plate. A stock solution was prepared for 50 μM Hsp90α protein. The Mosquito Crystallization Robot (SPT Labtech) was employed to dispense an ultra-low volume of Hsp90α proteins (750 nL per drop) on a 96-well hanging-drop film (FAstal BioTech, China, CAS: 296), followed by mixing

with 1 : 1 profiling solution. Subsequently, the 96-well film was inverted and adhered to a custom-made transparent, flat acrylic board or the back flat surface of a 96-well plate (Thermo Scientific, CAS: 167008). An optical microscope was employed for preliminary observation by monitoring the wells. The automatic imaging system of Operetta CLS high-content analysis system (PerkinElmer) was subsequently utilized to automatically scan and counts the number of droplets particles in each well. And each well would be scored based on the density and size of the droplets. For the protein phase separation score (PPS), 96 conditions were classified into 15 subzones (n1: A1–F1; n2: A2–F2; n3: A3–F3; n4: A4–F4; n5: A5–F5; n6: A6–F6; n7: A7–F7; n8: A8–F8; n9: A9–F9; n10: A10–F10; n11: A11–C12; n12: D11–F12; n13: G1–H5; n14: G6–H10; and n15: G11–H12). The value of each well in the subzone were averaged to obtain the score for each respective subzone (n1, n2, …, n15). The PPS score was calculated as the sum of the scores for each subzone. PPS of Hsp90α was calculated based on the equation (where $n$ indicates the serial number of the subzone):

$$\mathrm{pps}_{\mathrm{score}} = \sum_{n=1}^{15} \mathrm{subzone}\ \overline{n}$$

### *In vitro* phase separation assay

For the *in vitro* assessment of protein phase separation, the prepared protein solution was loaded onto a glass-bottom dish (80100, NEST) subsequent to the initiation of phase separation under specified experimental conditions. Imaging was performed using a Leica TCS SP8 microscope equipped with a 100× oil immersion objective. Both DIC and confocal microscopy images were captured at room temperature to analyze the phase separation dynamics.

### Fluorescence recovery after photobleaching assay

FRAP assay was performed using the FRAP module of the Leica SP8 confocal microscopy system using 100× oil objective (NA = 1.4). An aliquot of 10 μL pre-mixed sample was applied to a glass-bottom dish (80100, NEST). Fluorescence signals were bleached using a 100% intensity laser beam, and the bleaching area was set as the same diameter (1.2 μm) at the droplet with similar size. After photobleaching, images were continuously captured (2.65 s per image). For each time point, the fluorescence intensity was corrected by the intensity of a neighboring unbleached region. Image J and Prism 9 were applied to analyze the FRAP data.

### Cell cultures and cell lysates preparation

HeLa cells (TCHu187) were purchased from the cell bank of the Chinese Academy of Sciences, Shanghai. Cells were cultured in Dulbecco's Modified Eagle Medium (21013024, Gibco) supplemented with 10% (v/v) fetal bovine serum (10099141, Gibco) and 1% penicillin/streptomycin (15070063, Giboco) at 37 °C with 5% $CO_2$. To prepare cell lysates, cells were grown to confluency in 10 cm cell culture-treated dishes (150468, Thermo Fisher). To harvest cells, medium was aspirated and cells were washed with PBS. 1 mL lysis buffer (P0013B, Beyotime Biotechnology) containing proteinase inhibitor cocktail (5892970001, Roche) was added to the dish. After incubation for 15 min, the cell lysates were collected and centrifuged at centrifuged at 12 000*g* for 20 min to remove the debris. The protein concentration of the cell lysate was measure by BCA kit (23225, Thermo Fisher).

### Induction of LLPS in cell lysates and LC-MS/MS analysis

Hsp90α condensation was induced by adding 20 μM of Hsp90α and 10% PEG 8000 to the cell lysates (1 mg $mL^{-1}$). Granules were allowed to form for 40 min, and further isolated from the lysate by centrifugation at 2000*g* for 5 min. For control group, the equal concentration of Hsp90α was introduced to the system without adding PEG 8000. The system was then incubated for 40 minutes. After incubation, the samples were centrifuged at 2000*g* for 5 minutes. Subsequently, an equal volume of supernatant was carefully removed, following the same procedure as for the Hsp90α condensation group. Before MS analysis, proteins were precipitated with pre-cooled acetone and incubated at −20 °C overnight. The pellet was resuspended in 8 M urea, and 100 mM Tris (pH 8.5). TCEP and IAA were added to reduce the disulfide bond with a final concentration of 5 mM and 10 mM, respectively. Before digestion, the final concentration of urea was diluted to 2 M. After that, trypsin was added and incubated at 37 °C for 12 h. The digested peptides were desalted by a homemade C18 column, and reconstituted by 0.1% formic acid before injection. The peptides were analyzed by online nanoflow liquid chromatography-tandem mass spectrometry (LC-MS/MS). The peptides were separated on a nano column (100 μm × 15 cm, C18, 1.9 μm, 120 Å) and further analyzed using an Orbitrap Fusion mass spectrometer. One full-scan mass spectrum (350–1500 $m/z$) at a resolution of 120 000 followed by HCD fragmentation and detection of the fragment ions (scan range auto) in Orbitrap at a 32% normalized collision energy was repeated continuously. The Espritz DisProt was used to predict the intrinsically disordered regions (IDRs) of the enriched proteins, and RG motifs within these IDRs were subsequently identified and quantified.

### Bio-layer interferometry (BLI)

The binding kinetics of the TDP-43, hnRNPA1, $PR_{20}$ and $GR_{20}$ to Hsp90α were measured by BLI on a ForteBio Octet RED96 system (Pall ForteBio LLC). Assays were performed at 37 °C in a 96-well black flat bottom plate (Greiner Bio-One) with orbital shaking at 1000 rpm in buffer containing 50 mM Tris, pH 7.5 and 100 mM NaCl. Hsp90α was immobilized onto Ni-NTA biosensors (Sartorius, 18-5101) and incubated with varying concentrations of analytes in solution. The kinetic experiments comprised 7 steps: (i) baseline acquisition: Ni-NTA biosensors were incubated in the assay buffer for 2 min; (ii) an autoinhibition step: the analytes were incubated with the biosensors for 2 min; (iii) second baseline acquisition (10 min); (iv) loading: the Hsp90α was loaded onto the surfaces of biosensors until the response value accumulates to 1.0 nm; (v) third

baseline acquisition (10 min); (vi) association: incubating biosensors with different concentrations of analytes for 3 min to measure $K_{on}$; (vii) dissociation: incubating biosensors with the assay buffer for 5 min to measure $K_{off}$. The resulting curves were corrected by subtracting the blank reference, then fitted to a global fit algorithm using a 1 : 1 binding assumption to determine the $K_D$ ($K_{off}/K_{on}$) by the ForteBio Data Analysis software 9.0.

## Data availability

All experimental data are provided in the ESI.†

## Author contributions

D. L., and C. L. designed the project. J. H., Y. L., and J. G. planned the experiments. H. D. performed the HiPPS experiment. C. S., and Y. Z. ran the mass spectrometry samples. L. Y., and T. L. helped analyze the LC-MS/MS data. All of the authors were involved in analyzing the data and contributed to manuscript discussion and editing. J. H., D. L., and C. L. wrote the manuscript.

## Conflicts of interest

The authors declare no conflict of interest.

## Acknowledgements

This work was supported by the National Natural Science Foundation (NSF) of China (82188101 and 32171236 to C. L.; 92353302 and 32170683 to D. L.), the Science and Technology Commission of Shanghai Municipality (STCSM) (Grant No. 22JC1410400 to C. L.), the Shanghai Pilot Program for Basic Research – Chinese Academy of Science, Shanghai Branch (Grant No. CYJ-SHFY-2022-005 to C. L.), the CAS Project for Young Scientists in Basic Research (Grant No. YSBR-095 to C. L.)

## References

1 Y. E. Kim, M. S. Hipp, A. Bracher, M. Hayer-Hartl and F. U. Hartl, Molecular chaperone functions in protein folding and proteostasis, *Annu. Rev. Biochem.*, 2013, **82**, 323–355.
2 H. Saibil, Chaperone machines for protein folding, unfolding and disaggregation, *Nat. Rev. Mol. Cell Biol.*, 2013, **14**, 630–642.
3 F. U. Hartl, A. Bracher and M. Hayer-Hartl, Molecular chaperones in protein folding and proteostasis, *Nature*, 2011, **475**, 324–332.
4 Q. Xu, Y. Ma, Y. Sun, D. Li, X. Zhang and C. Liu, Protein amyloid aggregate: structure and function, *Aggregate*, 2023, **4**, e333.
5 D. Li and C. Liu, Molecular rules governing the structural polymorphism of amyloid fibrils in neurodegenerative diseases, *Structure*, 2023, **31**, 1335–1347.
6 F. H. Schopf, M. M. Biebl and J. Buchner, The HSP90 chaperone machinery, *Nat. Rev. Mol. Cell Biol.*, 2017, **18**, 345–360.
7 J. Li, J. Soroka and J. Buchner, The Hsp90 chaperone machinery: conformational dynamics and regulation by co-chaperones, *Biochim. Biophys. Acta*, 2012, **1823**, 624–635.
8 L. B. Shelton, J. Koren 3rd and L. J. Blair, Imbalances in the Hsp90 Chaperone Machinery: Implications for Tauopathies, *Front. Neurosci.*, 2017, **11**, 724.
9 R. Rosenzweig, N. B. Nillegoda, M. P. Mayer and B. Bukau, The Hsp70 chaperone network, *Nat. Rev. Mol. Cell Biol.*, 2019, **20**, 665–680.
10 E. A. Craig and J. Marszalek, How Do J-Proteins Get Hsp70 to Do So Many Different Things?, *Trends Biochem. Sci.*, 2017, **42**, 355–368.
11 H. H. Kampinga and E. A. Craig, The HSP70 chaperone machinery: J proteins as drivers of functional specificity, *Nat. Rev. Mol. Cell Biol.*, 2010, **11**, 579–592.
12 M. E. Cheetham and A. J. Caplan, Structure, function and evolution of DnaJ: conservation and adaptation of chaperone function, *Cell Stress Chaperones*, 1998, **3**, 28–36.
13 R. Zhang, D. Malinverni, D. M. Cyr, P. L. Rios and N. B. Nillegoda, J-domain protein chaperone circuits in proteostasis and disease, *Trends Cell Biol.*, 2023, **33**, 30–47.
14 A. M. Cuervo and E. Wong, Chaperone-mediated autophagy: roles in disease and aging, *Cell Res.*, 2014, **24**, 92–104.
15 M. S. Hipp, P. Kasturi and F. U. Hartl, The proteostasis network and its decline in ageing, *Nat. Rev. Mol. Cell Biol.*, 2019, **20**, 421–435.
16 Z. Albakova, Y. Mangasarova and A. Sapozhnikov, Heat Shock Proteins in Lymphoma Immunotherapy, *Front. Immunol.*, 2021, **12**, 660085.
17 A. Bohush, P. Bieganowski and A. Filipek, Hsp90 and Its Co-Chaperones in Neurodegenerative Diseases, *Int. J. Mol. Sci.*, 2019, **20**, 4976.
18 M. Zhang, C. Qian, Z. G. Zheng, F. Qian, Y. Wang, P. M. Thu, X. Zhang, Y. Zhou, L. Tu, Q. Liu, H. J. Li, H. Yang, P. Li and X. Xu, Jujuboside A promotes Aβ clearance and ameliorates cognitive deficiency in Alzheimer's disease through activating Axl/HSP90/PPARγ pathway, *Theranostics*, 2018, **8**, 4262–4278.
19 D. Li and C. Liu, Spatiotemporal dynamic regulation of membraneless organelles by chaperone networks, *Trends Cell Biol.*, 2022, **32**, 1–3.
20 J. Gu, Z. Liu, S. Zhang, Y. Li, W. Xia, C. Wang, H. Xiang, Z. Liu, L. Tan, Y. Fang, C. Liu and D. Li, Hsp40 proteins phase separate to chaperone the assembly and maintenance of membraneless organelles, *Proc. Natl. Acad. Sci. U. S. A.*, 2020, **117**, 31123–31133.
21 H. Zhang, X. Ji, P. Li, C. Liu, J. Lou, Z. Wang, W. Wen, Y. Xiao, M. Zhang and X. Zhu, Liquid-liquid phase separation in biology: mechanisms, physiological functions and human diseases, *Sci. China: Life Sci.*, 2020, **63**, 953–985.
22 H. Yu, S. Lu, K. Gasior, D. Singh, S. Vazquez-Sanchez, O. Tapia, D. Toprani, M. S. Beccari, J. R. Yates 3rd, S. Da Cruz, J. M. Newby, M. Lafarga, A. S. Gladfelter, E. Villa and D. W. Cleveland, HSP70 chaperones RNA-free TDP-43 into

anisotropic intranuclear liquid spherical shells, *Science*, 2021, **371**, 6529.

23 J. Gu, C. Wang, R. Hu, Y. Li, S. Zhang, Y. Sun, Q. Wang, D. Li, Y. Fang and C. Liu, Hsp70 chaperones TDP-43 in dynamic, liquid-like phase and prevents it from amyloid aggregation, *Cell Res.*, 2021, **31**, 1024–1027.

24 Y. Li, J. Gu, C. Wang, J. Hu, S. Zhang, C. Liu, S. Zhang, Y. Fang and D. Li, Hsp70 exhibits a liquid-liquid phase separation ability and chaperones condensed FUS against amyloid aggregation, *iScience*, 2022, **25**, 104356.

25 L. Mediani, F. Antoniani, V. Galli, J. Vinet, A. D. Carra, I. Bigi, V. Tripathy, T. Tiago, M. Cimino, G. Leo, T. Amen, D. Kaganovich, C. Cereda, O. Pansarasa, J. Mandrioli, P. Tripathi, D. Troost, E. Aronica, J. Buchner, A. Goswami, J. Sterneckert, S. Alberti and S. Carra, Hsp90-mediated regulation of DYRK3 couples stress granule disassembly and growth via mTORC1 signaling, *EMBO Rep.*, 2021, **22**, e51740.

26 T. R. O'Meara, M. J. O'Meara, E. J. Polvi, M. R. Pourhaghighi, S. D. Liston, Z. Y. Lin, A. O. Veri, A. Emili, A. C. Gingras and L. E. Cowen, Global proteomic analyses define an environmentally contingent Hsp90 interactome and reveal chaperone-dependent regulation of stress granule proteins and the R2TP complex in a fungal pathogen, *PLoS Biol.*, 2019, **17**, e3000358.

27 J. M. Pare, N. Tahbaz, J. López-Orozco, P. LaPointe, P. Lasko and T. C. Hobman, Hsp90 regulates the function of argonaute 2 and its recruitment to stress granules and P-bodies, *Mol. Biol. Cell*, 2009, **20**, 3273–3284.

28 Y. Li, J. Gu, C. Liu and D. Li, A high-throughput method for exploring the parameter space of protein liquid-liquid phase separation, *Cell Rep. Phys. Sci.*, 2022, **3**, 100764.

29 C. Hou, X. Wang, H. Xie, T. Chen, P. Zhu, X. Xu, K. You and T. Li, PhaSepDB in 2022: annotating phase separation-related proteins with droplet states, co-phase separation partners and other experimental information, *Nucleic Acids Res.*, 2023, **51**, D460–d465.

30 F. Gasset-Rosa, S. Lu, H. Yu, C. Chen, Z. Melamed, L. Guo, J. Shorter, S. Da Cruz and D. W. Cleveland, Cytoplasmic TDP-43 De-mixing Independent of Stress Granules Drives Inhibition of Nuclear Import, Loss of Nuclear TDP-43, and Cell Death, *Neuron*, 2019, **102**, 339–357.

31 A. Molliex, J. Temirov, J. Lee, M. Coughlin, A. P. Kanagaraj, H. J. Kim, T. Mittag and J. P. Taylor, Phase separation by low complexity domains promotes stress granule assembly and drives pathological fibrillization, *Cell*, 2015, **163**, 123–133.

32 I. R. A. Mackenzie, R. Rademakers and M. Neumann, TDP-43 and FUS in amyotrophic lateral sclerosis and frontotemporal dementia, *Lancet Neurol.*, 2010, **9**, 995–1007.

33 M. Grossman, W. W. Seeley, A. L. Boxer, A. E. Hillis, D. S. Knopman, P. A. Ljubenov, B. Miller, O. Piguet, R. Rademakers, J. L. Whitwell, H. Zetterberg and J. C. van Swieten, Frontotemporal lobar degeneration, *Nature Reviews Disease Primers*, 2023, **9**, 40.

34 A. F. Harrison and J. Shorter, RNA-binding proteins with prion-like domains in health and disease, *Biochem. J.*, 2017, **474**, 1417–1438.

35 H. J. Kim, N. C. Kim, Y. D. Wang, E. A. Scarborough, J. Moore, Z. Diaz, K. S. MacLea, B. Freibaum, S. Li, A. Molliex, A. P. Kanagaraj, R. Carter, K. B. Boylan, A. M. Wojtas, R. Rademakers, J. L. Pinkus, S. A. Greenberg, J. Q. Trojanowski, B. J. Traynor, B. N. Smith, S. Topp, A. S. Gkazi, J. Miller, C. E. Shaw, M. Kottlors, J. Kirschner, A. Pestronk, Y. R. Li, A. F. Ford, A. D. Gitler, M. Benatar, O. D. King, V. E. Kimonis, E. D. Ross, C. C. Weihl, J. Shorter and J. P. Taylor, Mutations in prion-like domains in hnRNPA2B1 and hnRNPA1 cause multisystem proteinopathy and ALS, *Nature*, 2013, **495**, 467–473.

36 S. Boeynaems, E. Bogaert, D. Kovacs, A. Konijnenberg, E. Timmerman, A. Volkov, M. Guharoy, M. De Decker, T. Jaspers, V. H. Ryan, A. M. Janke, P. Baatsen, T. Vercruysse, R. M. Kolaitis, D. Daelemans, J. P. Taylor, N. Kedersha, P. Anderson, F. Impens, F. Sobott, J. Schymkowitz, F. Rousseau, N. L. Fawzi, W. Robberecht, P. Van Damme, P. Tompa and L. Van Den Bosch, Phase Separation of C9orf72 Dipeptide Repeats Perturbs Stress Granule Dynamics, *Mol. Cell*, 2017, **65**, 1044–1055.

37 G. Kim, O. Gautier, E. Tassoni-Tsuchida, X. R. Ma and A. D. Gitler, ALS Genetics: Gains, Losses, and Implications for Future Therapies, *Neuron*, 2020, **108**, 822–842.

38 M. Wojciechowska, M. Olejniczak, P. Galka-Marciniak, M. Jazurek and W. J. Krzyzosiak, RAN translation and frameshifting as translational challenges at simple repeats of human neurodegenerative disorders, *Nucleic Acids Res.*, 2014, **42**, 11849–11864.

39 Y. Lin, E. Mori, M. Kato, S. Xiang, L. Wu, I. Kwon and S. L. McKnight, Toxic PR Poly-Dipeptides Encoded by the C9orf72 Repeat Expansion Target LC Domain Polymers, *Cell*, 2016, **167**, 789–802.

40 K. H. Lee, P. Zhang, H. J. Kim, D. M. Mitrea, M. Sarkar, B. D. Freibaum, J. Cika, M. Coughlin, J. Messing, A. Molliex, B. A. Maxwell, N. C. Kim, J. Temirov, J. Moore, R. M. Kolaitis, T. I. Shaw, B. Bai, J. Peng, R. W. Kriwacki and J. P. Taylor, C9orf72 Dipeptide Repeats Impair the Assembly, Dynamics, and Function of Membrane-Less Organelles, *Cell*, 2016, **167**, 774–788.

41 K. Matsumoto, M. Minami, F. Shinozaki, Y. Suzuki, K. Abe, S. Zenno, S. Matsumoto and Y. Minami, Hsp90 is involved in the formation of P-bodies and stress granules, *Biochem. Biophys. Res. Commun.*, 2011, **407**, 720–724.

42 J. A. Kolhe, N. L. Babu and B. C. Freeman, The Hsp90 molecular chaperone governs client proteins by targeting intrinsically disordered regions, *Mol. Cell*, 2023, **83**, 2035–2044.

43 M. Johnston, M. C. Geoffroy, A. Sobala, R. Hay and G. Hutvagner, HSP90 protein stabilizes unloaded argonaute complexes and microscopic P-bodies in human cells, *Mol. Biol. Cell*, 2010, **21**, 1462–1469.

44 P. Thandapani, T. R. O'Connor, T. L. Bailey and S. Richard, Defining the RGG/RG motif, *Mol. Cell*, 2013, **50**, 613–623.

45 F. Galibert, J. Hérissé and G. Courtois, Nucleotide sequence of the EcoRI-F fragment of adenovirus 2 genome, *Gene*, 1979, **6**, 1–22.
46 W. Kruijer, F. M. van Schaik and J. S. Sussenbach, Structure and organization of the gene coding for the DNA binding protein of adenovirus type 5, *Nucleic Acids Res.*, 1981, **9**, 4439–4457.
47 M. A. Lischwe, R. G. Cook, Y. S. Ahn, L. C. Yeoman and H. Busch, Clustering of glycine and NG,NG-dimethylarginine in nucleolar protein C23, *Biochemistry*, 1985, **24**, 6025–6028.
48 R. L. Ochs, M. A. Lischwe, W. H. Spohn and H. Busch, Fibrillarin: a new protein of the nucleolus identified by autoimmune sera, *Biol. Cell*, 1985, **54**, 123–133.
49 P. A. Chong, R. M. Vernon and J. D. Forman-Kay, RGG/RG Motif Regions in RNA Binding and Phase Separation, *J. Mol. Biol.*, 2018, **430**, 4650–4665.
50 M. Hofweber, S. Hutten, B. Bourgeois, E. Spreitzer, A. Niedner-Boblenz, M. Schifferer, M. D. Ruepp, M. Simons, D. Niessing, T. Madl and D. Dormann, Phase Separation of FUS Is Suppressed by Its Nuclear Import Receptor and Arginine Methylation, *Cell*, 2018, **173**, 706–719.
51 Q. Wang, Z. Li, S. Zhang, Y. Li, Y. Wang, Z. Fang, Y. Ma, Z. Liu, W. Zhang, D. Li, C. Liu and M. Ye, Global profiling of arginine dimethylation in regulating protein phase separation by a steric effect-based chemical-enrichment method, *Proc. Natl. Acad. Sci. U. S. A.*, 2022, **119**, e2205255119.
52 J. Song, Molecular mechanisms of phase separation and amyloidosis of ALS/FTD-linked FUS and TDP-43, *Aging Dis.*, 2024, **15**, 1118.
53 S. Lu, J. Hu, O. A. Arogundade, A. Goginashvili, S. Vazquez-Sanchez, J. K. Diedrich, J. Gu, J. Blum, S. Oung, Q. Ye, H. Yu, J. Ravits, C. Liu, J. R. Yates 3rd and D. W. Cleveland, Heat-shock chaperone HSPB1 regulates cytoplasmic TDP-43 phase separation and liquid-to-gel transition, *Nat. Cell Biol.*, 2022, **24**, 1378–1393.